Energy Management Design in Hybrid Electric Vehicles: A Novel Optimality and Stability Framework

Roberto Mura, *Student Member, IEEE*, Vadim Utkin, *Fellow, IEEE*, and Simona Onori, *Member, IEEE*

***Abstract*— This paper addresses the problem of finding a closed-form optimal solution for the energy management problem in charge-sustaining hybrid electric vehicles (HEVs), and proposes, for the first time, a generalized stability and optimality framework for this type of problem. The energy management problem, which by its very nature is a finite-time horizon control problem, is reformulated as a nonlinear–nonquadratic infinite-time optimization problem, leading to a family of state-feedback control laws that provide optimality with respect to an infinite time horizon performance objective, while guaranteeing asymptotic stability. The stability problem in charge-sustaining HEVs is formulated to allow the design of analytical solutions using a Lyapunov-based argument. The proposed control law is implemented on a pre-transmission parallel hybrid heavy-duty vehicle and the performance of the closed-loop system is shown in simulation and compared with the benchmark solution provided by Pontryagin's minimum principle (PMP) and the real-time adaptive controller adaptive-PMP. Results show low sensitivity to the control parameter, low-calibration effort, and reduction of computational effort, while maintaining close-to-the-optimum performance. Hardware-in-the-loop simulations were conducted to validate and verify the new strategy in a real-time simulation setup.**

***Index Terms*— Closed-form solution, energy management, hardware-in-the-loop (HIL), hybrid electric vehicles (HEVs), Lyapunov stability, optimal control, Pontryagin's minimum principle (PMP), supervisory control.**

I. Introduction

HYBRID electric vehicles (HEVs) encompass two (or more) energy storage sources and associated energy converters. Typically, the architecture of these vehicles includes an internal combustion engine with an associated fuel tank and one or more electric machine(s), requiring a battery system to store electrical energy [1]. The presence of an additional (or more) energy storage device gives rise to new degrees of freedom, since at each time the total power request for moving the vehicle can be delivered by either one of the on-board energy sources or their combination. With the additional degrees of freedom comes the problem of finding the most efficient way of splitting the power demand between the engine and the battery. The energy management system (EMS) is the control layer in the hybrid vehicle to which this task is demanded [2]–[6].

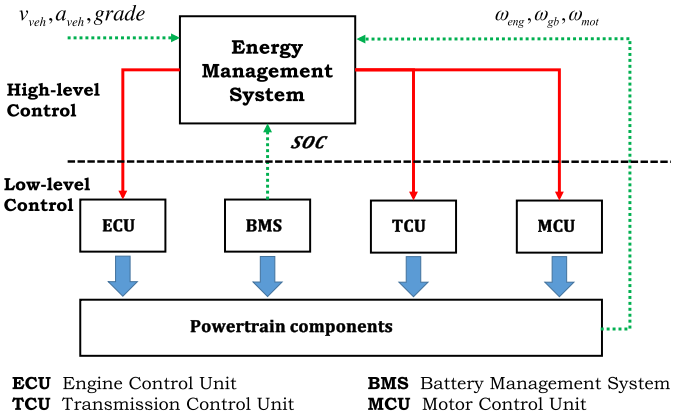

Fig. 1. Two-level control scheme in a hybrid vehicle.

Controlling an HEV generally includes two sets of tasks. One is the low-level control, where each powertrain component is controlled using classical feedback control methods [7]. The other task, referred to as high-level control, is responsible for the optimization of the energy flow on-board of the vehicle, while maintaining the battery state of charge within a certain range of operation. This layer of control, called EMS, receives and processes information from the powertrain (engine speed, ω_{eng}, gearbox speed, ω_{gb}, and electric motor speed, ω_{mot}) and the actual driving cycle (Cyc) (vehicle speed, v_{veh}, vehicle acceleration, a_{veh}, and grade) and outputs the optimal actuator setpoints which are executed by the low-level control. The two-task-based control scheme in an HEV is shown in Fig. 1. This paper[1] presents a new theoretical framework and its hardware-in-the-loop (HIL) implementation of a closed-form optimal and stable energy management strategy for EMS implementation in an HEV.

This paper is structured as follows. In Section II, a classification and review of the main methods proposed in the literature for EMS design is presented. This leads to the main

Manuscript received November 27, 2013; revised June 24, 2014; accepted August 16, 2014. Manuscript received in final form October 11, 2014. Recommended by Associate Editor L. Del Re.

R. Mura was with the Center for Automotive Research, Columbus, OH 43212 USA. He is now with the Dipartimento di Elettronica, Informazione e Bioingegneria, Politecnico di Milano, Milan 20133, Italy (e-mail: roberto.mura@polimi.it).

V. Utkin is with the Department of Electrical Engineering, Ohio State University, Columbus, OH 43210 USA (e-mail: utkin@ece.osu.edu).

S. Onori is with the Department of Automotive Engineering, Clemson University, Clemson, SC 29634 USA (e-mail: sonori@clemson.edu).

Color versions of one or more of the figures in this paper are available online at http://ieeexplore.ieee.org.

Digital Object Identifier 10.1109/TCST.2014.2363617

[1]Preliminary results related to this research appeared in [8].

motivation of this paper. Section III describes the hybrid vehicle model used in this paper. In Section IV, the energy management problem as a constrained optimization problem over a finite-time horizon is reviewed. In Section V, the novel energy management framework is presented and the infinite-time optimization and stability idea introduced. In Section VI, the novel nonlinear-optimal control strategy (NL-OCS) is designed. Pontryagin's minimum principle (PMP) and its adaptive-version PMP (A-PMP) are reviewed in Section VII. A sensitivity study over the new control law parameters and comparison with PMP and A-PMP is conducted in Section VIII. The HIL setup is discussed in Section IX along with HIL strategy implementation. The conclusion is included in Section X.

II. Review of Energy Management Strategies for HEVs

Several families of energy management strategies have been proposed in the literature over the past 15 years. Two general trends can be identified that deal with this problem, namely, heuristics methods and model-based optimization solutions [9]–[11].

A. Heuristics Methods

The simplest way to deal with the energy management problem, which does not involve explicit optimization, is by designing rules to manage the on-board energy of the vehicle [12], [13]. The main advantage of this class of approaches is their effectiveness in real-time implementation, whereas their disadvantage is a large calibration set of parameters requiring *ad hoc* tuning. Rules are generally designed based on heuristics, intuition [14] or from the knowledge of optimal global solution generated with mathematical models through optimization algorithms [15]–[19].

B. Model-Based Methods

To fully exploit the potential of hybrid architectures, model-based optimal control methods were started being successfully used over the last decade.

Optimal model-based techniques generate noncasual solutions in that they find the minimum value of a cost function using knowledge of the future driving information. Although these control methods cannot be used directly for real-time implementation they constitute a valuable design tool in that they are sometime the basis to design rules for online implementation or used as a benchmark solution to evaluate the performances of other control strategies.

We can divide model-based optimization methods into numerical and analytical approaches. In numerical optimization methods, like dynamic programming [20], simulated annealing [21], and genetic algorithms [22] the complete knowledge of the driving mission is used and the global optimum is found numerically.

Analytical optimization methods, on the other hand, use a mathematical problem formulation to find an analytical solution or at least provide an analytical formulation that makes the numerical solution faster than the purely numerical methods. Among these methods, PMP has been the most successfully implemented [23]. Equivalent consumption minimization strategy (ECMS) can be also enumerated within this category, as only quite recently it has been shown to be equivalent to the PMP method [24].

Both DP, PMP, and ECMS methods can only generate an optimal solution if implemented offline [25].

For online implementation other model-based methods have been explored and proposed that lead to suboptimal solutions.

When information about past and present driving conditions is used, and/or prediction of future driving conditions may be used then model predictive control (MPC) and stochastic dynamic programming were shown to be good candidates to generate suboptimal power split laws [4], [26]–[30].

When MPC is used [28], [31]–[34], a short-term optimization horizon in the future is considered during which the driving Cyc is predicted and the optimal power split is found. One of the main drawbacks of this approach is the high-computational power required to solve the minimization at each sampling interval. To overcome this drawback, Fast-MPC has been proposed that calculates the entire solution domain offline [35]–[37]. In our opinion, the application of MPC or Fast-MPC in solving the traditional energy management problem in HEVs (as defined in Section IV) is a technology overkill. On the other hand, MPC is found to be a helpful and promising technique when used, for example, to smoothing out the engine transient behavior in HEVs [38].

C. Motivation

Within the model-based techniques discussed, local optimization methods, such as PMP and ECMS, have been the preferred path to go in designing EMS, in that they can guarantee, under given conditions, near-optimal performance, while minimizing an instantaneous cost [24], [39]–[42].

The main idea underneath is that a virtual fuel consumption can be associated with the use of electrical energy and summed to the actual fuel consumed. The sum of the two, i.e., total equivalent fuel consumption, is then being optimized instantaneously. In the optimal control theory language, this total equivalent fuel consumption function is called Hamiltonian [24].

Both ECMS and PMP require some parameters to be tuned, namely, the equivalence factors (s_{ch} and s_{dsh}) for ECMS and costate (λ) for PMP. These are found offline for each driving Cyc. These parameters can be interpreted as the average efficiency of the electric path during a charge or discharge condition for a given driving mission. Hence, optimality is only achieved when future driving information is known, thus making them not suitable candidates for in-vehicle implementation.

For that, online adaptation of the tuning parameters as driving scenarios change was proposed in the form of adaptive-ECMS or A-PMP [34], [43]–[45], where an autoregressive moving average filter or PI-like adaptive law was used for online adaptation.

The operation of minimizing the Hamiltonian on-board of the vehicle at each tick of the clock, aside form being

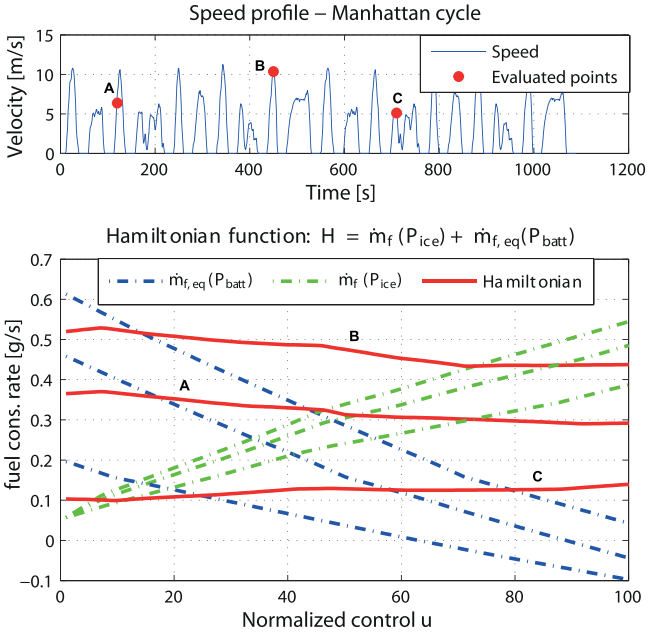

Fig. 2. Hamiltonian function $\mathcal{H}$ (bottom) evaluated for different instances of a Manhattan driving Cyc (top). The Hamiltonian accounts for two terms: fuel consumption rate $\dot{m}_f(P_{\text{ice}})$ and the virtual electric equivalent consumption $\dot{m}_{f,\text{eq}}(P_{\text{batt}})$.

computationally expensive, can lead in some cases to unpredictable results, due to the fact that this function might be in some instances of the driving Cyc not a convex function of the control variable or have local minima. This can be noticed in Fig. 2, where the Hamiltonian function is plotted for three different instances of the driving Cyc. Nonuniqueness of the control signal selection during the minimization process, could lead to abrupt changes in the control outputs [46].

Motivated by these issues, a new model-based strategy is proposed in this paper. Inspired by Bernstein's work [47] on theoretical results on optimal nonlinear regulation problem involving non quadratic cost functionals, a first attempt to propose a new control framework for the energy management problem was given in [48]. The authors cast the energy management problem into a nonlinear optimal regulation problem, where the battery state of charge was optimally regulated to its reference target in the case of zero disturbance. Preliminary results showed the feasibility of the closed-form control law in the simple case of vehicle at standstill. Reduction in computational execution and decreased sensitivity of the control parameter with respect to driving conditions were also showed. Nonetheless, two issues were not being addressed properly in [48]: 1) the definition of stability and 2) the extension of the finite-time cost function into an infinite-time functional (needed to fully use results from [47] and [49]).

Based on these premises, this paper proposes an extension and improvement of concepts initially presented in [48] and [50]. The objective is to find an analytical, closed-form, energy management strategy suited for in-vehicle implementation, while assuring optimality and stability. To this end, the problem is cast into a nonlinear infinite-time optimal regulation problem, and a Lyapunov-based approach is used

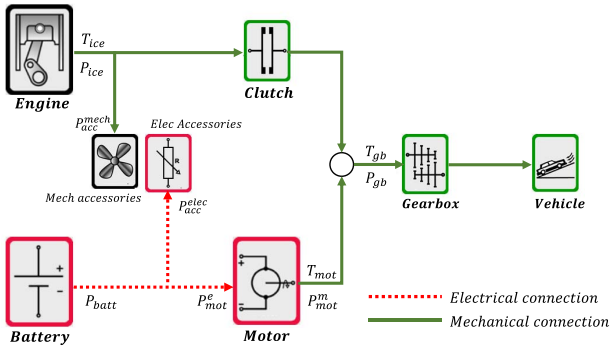

Fig. 3. Power flow diagram of pre-transmission parallel HEVs.

TABLE I
VEHICLE CHARACTERISTICS

Vehicle mass	19878 kg
Engine power	194 kW
Motor power	200 kW
Battery energy capacity	7.5 kWh
Electrical accessory	7 kW
Mechanical accessory	4 kW

to design an analytical control law, which produces closed-loop performances comparable with the benchmark solutions provided by PMP.

III. HYBRID HEAVY-DUTY TRUCK MODEL

The vehicle model used in this paper is a heavy duty pre-transmission parallel HEV, whose schematic is shown in Fig. 3. The engine, connected in parallel with the electric motor, can be engaged or disengaged from the wheels through a clutch. The vehicle can operate in three different modes, which are described in the following, depending on the status of the clutch and the gear position.

The characteristics of the vehicle are shown in Table I.

A. Electric Mode

In this mode, the clutch is open and the vehicle uses only the battery and the electric motor for propulsion; the engine is not connected to the wheels and is switched OFF. Since there is just one propulsion device in this mode the torque/power requested by the driver at the wheels is totally satisfied using the electric drivetrain and no optimization is needed. The instantaneous torque/power balance equations are

$$\begin{cases} T_{\text{mot}}(t) = T_{\text{gb}}(t) \\ P_{\text{batt}}(t) = P^e_{\text{mot}}(t) + P^e_{\text{acc}} \\ \omega_{\text{mot}}(t) = \omega_{\text{gb}}(t) \end{cases} \qquad \forall t \in [0,\ T] \tag{1}$$

where $T_{\text{gb}}(t)$ and $\omega_{\text{gb}}(t)$ are the instantaneous gearbox torque and speed; $P_{\text{batt}}(t)$ is the battery power; $T_{\text{mot}}(t)$ and $\omega_{\text{mot}}(t)$ are the instantaneous electric motor torque and speed; P^e_{acc} represents the electrical accessory power (considered constant) and $P^e_{\text{mot}}(t)$ represents the instantaneous electrical power of the electric motor. Moreover

$$P^m_{\text{mot}} = \begin{cases} \eta_{\text{mot}} \cdot P^e_{\text{mot}} & P^e_{\text{mot}} > 0 \\ \dfrac{1}{\eta_{\text{mot}}} \cdot P^e_{\text{mot}} & P^e_{\text{mot}} < 0 \end{cases} \tag{2}$$

where $P^m_{\text{mot}}(t)$ and η_{mot} are the instantaneous electric motor mechanical power and the efficiency, respectively.

B. Parallel Mode With Neutral Gear

This mode of operation occurs when the vehicle is at standstill with the clutch closed and the gearbox in neutral position. The engine is still connected to the transmission, but its speed is free to vary as the gearbox is in neutral position. The instantaneous torque, power, and speed balance equations to be satisfied are

$$\begin{cases} T_{\text{ice}}(t) - T^m_{\text{acc}}(t) = -T_{\text{mot}}(t) \\ P_{\text{batt}}(t) = P^e_{\text{mot}}(t) + P^e_{\text{acc}} \\ \omega_{\text{mot}}(t) = \omega_{\text{ice}}(t) = \omega^*_{\text{ice}}(t) \end{cases} \quad \forall t \in [0,\ T] \tag{3}$$

where $T_{\text{ice}}(t)$ and $\omega_{\text{ice}}(t)$ are the instantaneous engine torque and speed; $T^m_{\text{acc}}(t)$ is the instantaneous mechanical accessory torque; and $\omega^*_{\text{ice}}(t)$ represents the instantaneous optimal engine speed obtained by selecting the maximum efficiency operating line of the engine [see (16) in Section IV-A for more details]. Being the total power requested at the wheels zero, the power balance equations can be written as

$$P_{\text{gb}}(t) = 0 = P_{\text{ice}}(t) - P^m_{\text{acc}}(t) + \frac{1}{\eta_{\text{mot}}} \cdot \left(P_{\text{batt}}(t) - P^e_{\text{acc}}\right). \tag{4}$$

C. Parallel

In this mode both devices are used for propulsion, with clutch closed and the engine connected to the wheels. The speed at the wheels determines, through the transmission, the speed of both the electric machine and the engine. The powertrain equations are

$$\begin{cases} T_{\text{ice}}(t) - T^m_{\text{acc}} + T_{\text{mot}}(t) = T_{\text{gb}}(t) \\ P_{\text{batt}}(t) = P^e_{\text{mot}}(t) + P^e_{\text{acc}} \\ \omega_{\text{mot}}(t) = \omega_{\text{ice}}(t) = \omega_{\text{gb}}(t). \end{cases} \quad \forall t \in [0,\ T] \tag{5}$$

Hence

$$P_{\text{gb}} = \begin{cases} P_{\text{ice}} - P^m_{\text{acc}} + \eta_{\text{mot}} \cdot \left(P_{\text{batt}} - P^e_{\text{acc}}\right) & P^e_{\text{mot}} > 0 \\ P_{\text{ice}} - P^m_{\text{acc}} + \dfrac{1}{\eta_{\text{mot}}} \cdot \left(P_{\text{batt}} - P^e_{\text{acc}}\right) & P^e_{\text{mot}} < 0. \end{cases} \tag{6}$$

The vehicle model described above has been implemented into a detailed forward model simulator Powertrain Simulation Analysis Toolkit (PSAT) [51]. PSAT is a state-of-the-art flexible powertrain simulation software developed by Argonne National Laboratory, running in MATLAB/Simulink environment, which provides access to dynamic models of different mechanical and electrical components of several hybrid vehicle configurations [52], [53]. The level of details in PSAT component models and its forward simulation approach ensures reliable estimation of the fuel economy [53].

IV. Energy Management Problem-Classical Formulation

The objective of the energy management strategy in an HEV is to find the optimal power split between the primary and secondary energy sources that minimizes a given objective function over an entire driving Cyc. In particular, the aim is to minimize the total mass of fuel m_f [g] during a driving mission of length T, starting from $t = 0$. This is equivalent to minimize the cost J_T

$$J_T = \int_0^T L(u(t))dt \tag{7}$$

where $L(u(t)) = \dot{m}_f(u(t))$ is the instantaneous fuel consumption rate expressed in [g/s] and $u(t)$ is the control variable.

When solving the energy management problem, usually the only state variable is the battery SOC$(\cdot)$, whose dynamics is defined as

$$\dot{\text{SOC}}(t) = -\eta_{\text{batt}} \frac{I(t)}{Q_{\text{max}}} \tag{8}$$

where η_{batt} represents the battery efficiency, $I(t)$ [A] the actual battery current (positive in discharging and negative in charging) and Q_{max} [Ah] the maximum battery capacity. In a charge-sustaining HEV, the net energy variation in the battery over a given driving Cyc should be zero. This condition is guaranteed by imposing that the SOC is the same at the beginning and at the end of the Cyc

$$\text{SOC}(0) = \text{SOC}(T) = \text{SOC}_{\text{ref}}. \tag{9}$$

Equation (9) represents the global constraints of the optimal problem.

Local constraints are imposed on state and control variables as well. These constraints mostly concern physical operation limits, such as maximum engine torque and speed, maximum motor power, and the battery SOC limits. For pre-transmission parallel HEV powertrain local constraints are expressed as

$$\begin{cases} P_{\text{batt,min}} \le P_{\text{batt}}(t) \le P_{\text{batt,max}} \\ \text{SOC}_{\text{min}} \le \text{SOC}(t) \le \text{SOC}_{\text{max}} \\ T_{x,\text{min}} \le T_x(t) \le T_{x,\text{max}} \\ P_{x,\text{min}} \le P_x(t) \le P_{x,\text{max}} \\ \omega_{x,\text{min}} \le \omega_x(t) \le \omega_{x,\text{max}} \end{cases} \quad \begin{array}{l} \\ \\ \forall t \in [0,\ T] \\ \\ x = \text{ice, mot} \end{array} \tag{10}$$

where the last three inequalities represent limitations on the instantaneous engine and motor torque, power (both mechanical and electrical for the electric motor), and speed, respectively; $(\cdot)_{\text{min}}$ and $(\cdot)_{\text{max}}$ are the minimum and maximum value of power/SOC/torque/speed at each instant. In particular, battery power limits are not constant but depend on internal parameters according to the following relations:

$$\begin{cases} P_{\text{batt,min}} = V_{\text{max}} \cdot \dfrac{V_{\text{oc}}(\text{SOC}) - V_{\text{min}}}{R_s} \\ P_{\text{batt,max}} = V_{\text{min}} \cdot \dfrac{V_{\text{max}} - V_{\text{oc}}(\text{SOC})}{R_s} \end{cases} \tag{11}$$

where V_{oc} [V] is the battery open circuit voltage that depends on SOC and R_s [Ω] is the battery internal resistance. Moreover, powertrain constraints are also enforced at each instant to ensure that the total power demand at the wheels is satisfied, in accordance to the specific mode of operation. Within this formulation the energy management problem can be defined as follows.

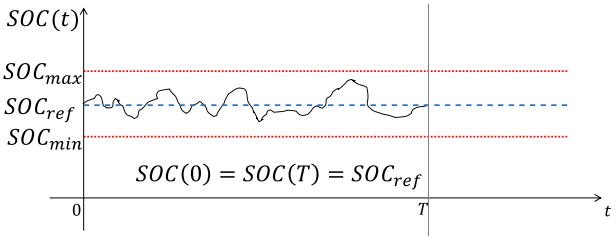

Fig. 4. SOC profile obtained solving the HEV energy management problem, as formulated in Problem 1.

Problem 1: The energy management problem in charge-sustaining HEVs consists in the minimization of the cost function (7) subject to system dynamics (8), global constraints (9), and local constraints (10).

We refer to Problem 1 as the standard HEV energy management problem. A typical solution, in terms of SOC behavior, resulting from solving Problem 1 is shown in Fig. 4.

A. Fuel Flow Rate Consumption-Engine Model

In the control design proposed in this paper we use a Willans line-based model for the engine fuel consumption, where the engine chemical power (P_{chem}) is given as a function of the engine power ($P_{\text{ice}} = T_{\text{ice}} \cdot \omega_{\text{ice}}$) and speed ($\omega_{\text{ice}}$)

$$P_{\text{chem}}(t) = e_0(\omega_{\text{ice}}(t)) + e_1(\omega_{\text{ice}}(t)) \cdot P_{\text{ice}}(t) \tag{12}$$

where $e_0(\omega)$ is the engine friction losses and $e_1(\omega)$ the conversion efficiency of the machine. A good approximation of the friction losses and conversion efficiency coefficients is given by expressing e_0 and e_1 as a quadratic fitting with respect to engine speed, as

$$\begin{cases} e_0(\omega_{\text{ice}}(t)) = e_{00} + e_{01} \cdot \omega_{\text{ice}}(t) + e_{02} \cdot \omega_{\text{ice}}^2(t) \\ e_1(\omega_{\text{ice}}(t)) = e_{10} + e_{11} \cdot \omega_{\text{ice}}(t) + e_{12} \cdot \omega_{\text{ice}}^2(t) \end{cases} \tag{13}$$

where $e_{ij} > 0$, $i, j = 0, 1, 2$ are the constant Willans line coefficients. Being the chemical engine power input $P_{\text{chem}} = \dot{m}_f \cdot Q_{\text{LHV}}$ (Q_{LHV} is the lower heating calorific value of diesel in [kJ/kg]) the fuel consumption rate can be written as

$$\dot{m}_f(t) = \frac{1}{Q_{\text{LHV}}}[e_0(\omega_{\text{ice}}(t)) + e_1(\omega_{\text{ice}}(t)) \cdot P_{\text{ice}}(t)]. \tag{14}$$

The effectiveness of the Willans line model in approximating the fuel consumption rate of the engine is shown in Fig. 5.

When the vehicle is operating in parallel mode with neutral gear, the Willans line model of the engine gives a means to calculate an analytical expression of the optimal engine speed. In this case, the engine speed ω_{ice} can be selected to optimize engine operation, by minimizing the chemical power P_{chem}

$$\begin{cases} \dfrac{\partial P_{\text{chem}}}{\partial \omega_{\text{ice}}} = 0 \\ \dfrac{\partial^2 P_{\text{chem}}}{\partial \omega_{\text{ice}}^2} > 0 \end{cases} \tag{15}$$

which, using (12) and (13), leads to

$$\omega_{\text{ice}}^*(t) = -\frac{1}{2} \cdot \frac{e_{01} + e_{11} P_{\text{ice}}(t)}{e_{02} + e_{12} P_{\text{ice}}(t)} \tag{16}$$

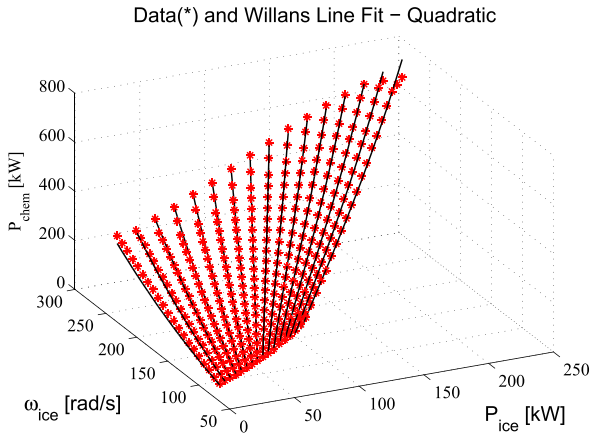

Fig. 5. Coefficients fitting of the Willans line model.

with $\omega_{\text{ice}}^*(t) \text{ı} [\omega_{\text{ice}}^{\text{idle}}, \omega_{\text{ice}}^{\text{max}}]$. In (16), $\omega_{\text{ice}}^*(t)$ is a function of the engine power requested for charging the battery pack (because in neutral gear mode).

Defining the new set of parameters p_0 and p_1 as

$$p_0(\omega_{\text{ice}}^*(t)) = \frac{e_0(\omega_{\text{ice}}^*(t))}{Q_{\text{LHV}}}$$
$$p_1(\omega_{\text{ice}}^*(t)) = \frac{e_1(\omega_{\text{ice}}^*(t))}{Q_{\text{LHV}}}$$

the fuel consumption rate model (14) can be either rewritten in terms of P_{ice} as

$$\dot{m}_f(t) = p_0(\omega_{\text{ice}}^*(t)) + p_1(\omega_{\text{ice}}^*(t)) P_{\text{ice}}(t) \tag{17}$$

or, using (4), it can be expressed as a function of P_{batt} as

$$\dot{m}_f = n_0(\omega_{\text{ice}}^*(t)) + n_1(\omega_{\text{ice}}^*(t)) P_{\text{batt}}(t) \tag{18}$$

where coefficients n_0 and n_1 are

$$n_0(\omega_{\text{ice}}^*(t)) = p_0(\omega_{\text{ice}}^*(t)) + p_1(\omega_{\text{ice}}^*(t)) \left(P_{\text{acc}}^{\text{mech}} + \frac{P_{\text{acc}}^{\text{elec}}}{\eta_{\text{mot}}} \right)$$
$$n_1(\omega_{\text{ice}}^*(t)) = -\frac{p_1}{\eta_{\text{mot}}}. \tag{19}$$

The Willans line fuel consumption rate model, together with a suitable description of the battery model, is used in the following section to reformulate the energy management problem as an infinite-time horizon optimal control problem including stability.

V. New Energy Management Framework

The novel approach proposed in this paper consists in rethinking the optimal control problem for HEV energy management (Problem 1) as a nonlinear–nonquadratic optimization problem over an infinite time horizon. In particular, a Lyapunov-based approach is used to design the controller, leading to a family of feedback closed-form control laws that guarantee stability and optimality with respect to an adjoint cost function. This adjoint cost (introduced later in this section and defined more formally in the Appendix) guarantees a bound on the worst case value of the nonquadratic cost functional over a prescribed set of bounded input disturbances.

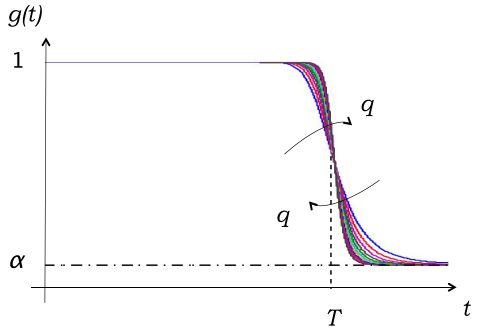

Fig. 6. Behavior of $g(t)$ for different values of q. Note that for $q \to \infty$ is obtained that $J_\infty = J_T + J_\alpha$ where J_T is defined in (7) and $J_\alpha = \int_T^\infty \dot{m}_f \cdot \alpha \, dt$.

To ensure optimality of vehicle operation when $t > T$, the $[0, \ T]$ optimization horizon is extended into the infinite horizon $[0, \infty]$, so as to lead to a new cost function defined over $[0, \ \infty]$

$$J_\infty = \int_0^\infty \dot{m}_f(u(t)) \cdot g(t) dt \tag{20}$$

by means of the scalar positive function $g(t)$, as shown in Fig. 6, and defined as

$$g(t) = \frac{1 + \alpha\left(\frac{t}{T}\right)^q}{1 + \left(\frac{t}{T}\right)^q} \qquad 0 < \alpha < 1, \quad q > 0 \tag{21}$$

whose role is to penalize the action of the control $u(t)$ for $t > T$ to approximate the finite-time cost J_T defined in (7) with the infinite-time functional (20).

In [47] and [49], it was shown that under certain conditions on the system and the cost function, nonlinear controllers offer advantages over linear ones, in particular, when the plant dynamics and/or system output are nonlinear, the performance measure is nonquadratic, or the control signals are constrained. In the following, the system is reformulated to fit the problem in the form presented in [49] (in the Appendix the main result from [49] is included for ease of presentation).

A. System Dynamics Reformulation

The battery state of energy (SOE), defined as the amount of battery energy stored at the present time ($E(t)$) to the maximum battery energy capacity ($E_{\max}$), is used as state variable in this discussion. SOE is related to SOC by the relation

$$\text{SOE}(t) = \text{SOC}(t)\frac{V_L(t)}{V_{\text{oc}}^{\max}} = \frac{E(t)}{E_{\max}} \tag{22}$$

where V_L is the battery terminal voltage and $V_{\text{oc}}^{\max}$ the maximum open circuit voltage. From here on the explicit dependence of time will be omitted. The SOE dynamics is

$$\begin{cases} \dot{\text{SOE}} = -\eta_{\text{batt}} \dfrac{P_{\text{batt}}}{E_{\max}} \\ E_{\max} = Q_{\max} \cdot V_{\text{oc}}^{\max}. \end{cases} \tag{23}$$

Assuming

$$k = \frac{\eta_{\text{batt}}}{E_{\max}\eta_{\text{mot}}} \tag{24}$$

the battery SOE error $\zeta = \text{SOE}_{\text{ref}} - \text{SOE}$ is introduced, whose dynamics is described as a function of the control input (P_{ice}) and the disturbance (P_{req}) by virtue of (6)

$$\dot{\zeta} = -k P_{\text{ice}} + k P_{\text{req}}. \tag{25}$$

Note that in parallel mode the power requested is the sum of mechanical and electrical accessory powers and the gearbox power. When the vehicle is not moving ($v = 0$), instead, the power requested P_{req} only accounts for the power accessory loads. The disturbance power, P_{req}, is thus expressed as

$$P_{\text{req}} = \begin{cases} P_{\text{gb}} + \eta_{\text{mot}} P_{\text{acc}}^e + P_{\text{acc}}^m & v > 0 \quad \forall t \in [0, \ T] \\ \eta_{\text{mot}} P_{\text{acc}}^e + P_{\text{acc}}^m & v = 0 \quad \forall t \in [T, \ \infty]. \end{cases} \tag{26}$$

Defined this way, the power request P_{req} is a $\mathcal{L}_2$ signal. Consider an open set $\mathcal{Z} \subset \mathbb{R}$ such that $\zeta \in \mathcal{Z}$, a set $\mathcal{U} \subset \mathbb{R}$ such that $P_{\text{ice}} \in \mathcal{U}$, and a set $\mathcal{W} \subset \mathbb{R}$ such that $P_{\text{req}} \in \mathcal{W}$ and P_{req} in $\mathcal{L}_2$. The domain of control, state, and disturbance variables are

$$\begin{cases} \mathcal{Z} = [\text{SOE}_{\text{ref}} - \text{SOE}_{\max}, \text{SOE}_{\text{ref}} - \text{SOE}_{\min}] \\ \mathcal{U} = \left[0, \ P_{\text{ice}}^{max}\right] \\ \mathcal{W} = \{P_{\text{req}} : P_{\text{req}} \in \mathcal{L}_2\}. \end{cases} \tag{27}$$

Then consider the following control system (where $\zeta = 0$ is an equilibrium point):

$$\begin{cases} \dot{\zeta} = -k P_{\text{ice}} + k P_{\text{req}}, \quad \zeta(0) = \zeta_0 \\ z = \zeta \end{cases} \tag{28}$$

where z is the performance variable, and the cost functional defined as

$$J_\infty(\zeta_0, P_{\text{ice}}(\cdot)) = \int_0^\infty \frac{(p_0(\omega_{\text{ice}}) + p_1(\omega_{\text{ice}}) \cdot P_{\text{ice}}(t)) \cdot g(t)}{Q_{\text{LHV}}} dt. \tag{29}$$

Problem 2: The infinite-time energy management optimal control problem consists in minimizing the cost function (29) under system dynamics (28), with state and control variables defined in $\mathcal{Z}$ and $\mathcal{U}$, respectively, and $P_{\text{req}} \in \mathcal{W}$.

Definition 1: Consider Problem 2 with $P_{\text{req}} \equiv 0$ and $\phi(\zeta(t))$ an optimal solution for the problem. Then, the origin $\zeta(t) = 0$ of the closed-loop system under $\phi(\zeta(t))$ is asymptotically stable if $\zeta(t) \to 0$ for $t \to \infty$.

When solving Problem 2 in the presence of P_{req} given by (26), a typical SOC behavior is shown in Fig. 7. It can be noticed that the global constraint (9) requiring $\text{SOC}(T)$ to be equal to the reference value SOC_{ref} is not met. In other words, different SOC values can be assumed at $t = T$, and the convergence to SOC_{ref} is guaranteed only as $t \to \infty$.

Following the lines of Theorem 2 (the Appendix), a Lyapunov-based approach is used to obtain a state-feedback control law to find the optimal torque/power split between the engine and the electric motor, where the power request P_{req} is regarded as a $\mathcal{L}_2$ disturbance.

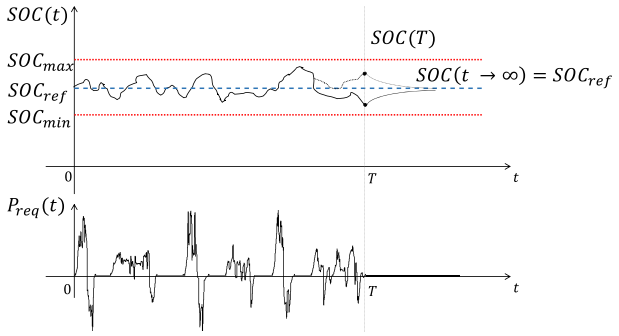

Fig. 7. Typical SOC trajectory obtained from solving Problem 2 (top) when P_{req} profile (bottom) is applied.

VI. Nonlinear Optimization Control Strategy (NL-OCS) Design

With respect to the system (28) the Hamiltonian function $\mathcal{H}$ (57) takes on the form [23]

$$\mathcal{H}(\zeta, P_{\text{ice}}, \lambda) = \dot{m}_f(P_{\text{ice}}) \cdot g(t) + \Gamma(\zeta, P_{\text{ice}}) + \lambda \cdot (-k P_{\text{ice}}) \quad (30)$$

where $\dot{m}_f$ is the instantaneous cost function and $\Gamma(\zeta, P_{\text{ice}})$ is a positive definite function of ζ and the control variable, and λ is the costate variable. To guarantee that the Hamiltonian function is zero at the minimum value, a shifting of the $\mathcal{H}$ is operated as follows:

$$\bar{\mathcal{H}}(\zeta, P_{\text{ice}}, \lambda) = \mathcal{H}(\zeta, P_{\text{ice}}, \lambda) - p_0(\omega_{\text{ice}}). \quad (31)$$

Theorem 1: Consider the system (28) with functional cost (29). Then, the feedback control law $P^*_{\text{ice}}(\zeta)$ defined as

$$P^*_{\text{ice}} = \phi(\zeta) = \begin{cases} \dfrac{2k^2(\mu^4\zeta^3)^2}{(k\mu^4\zeta^3 - p_1(\omega_{\text{ice}})\ g(t))\gamma^2} & \zeta > \bar{\zeta} \\ \zeta^2 & 0 < \zeta \le \bar{\zeta} \end{cases} \quad (32)$$

with $\bar{\zeta} = (p_1(\omega_{\text{ice}})/k\mu^4)^{1/3}$, μ positive gain and k as in (24), is such that:

1) the solution $\zeta(t) = 0$, $t \ge 0$ of the closed-loop system is locally asymptotically stable in accordance to Definition 1;
2) the adjoint performance functional (29)

$$J_\infty(\zeta_0, P_{\text{ice}}(\cdot)) = \int_0^\infty \frac{p_0(\omega_{\text{ice}}) + p_1(\omega_{\text{ice}}) \cdot P_{\text{ice}}(t)}{Q_{\text{LHV}}}\, dt \quad (33)$$

is minimized.

Note that when $\zeta < 0$ the control strategy switches to the pure electric mode.

Proof 1: Consider the candidate Lyapunov function

$$V(\zeta) = \frac{1}{4}\mu^4\zeta^4, \quad \mu \in R \quad (34)$$

then the storage function $\Gamma(\zeta, P_{\text{ice}})$ and the supply rate function $r(\zeta, P_{\text{req}})$, for the system (28) and the Lyapunov function (34), are defined as

$$\begin{cases} \Gamma(\zeta, P_{\text{ice}}) = \dfrac{1}{\gamma^2}\left(\dfrac{\partial V}{\partial \zeta}\right)^2 k^2 \cdot \left(1 + \log\left(P^2_{\text{ice}}\right)\right) \\ r(\zeta, P_{\text{req}}) = \gamma^2 P^2_{\text{req}} - \zeta^2. \end{cases} \quad (35)$$

To proves 1 and 2 of Theorem 1, the set of sufficient conditions from Theorem 2 (in the Appendix) are shown to hold true with the optimal feedback control $\phi(\zeta) = P^*_{\text{ice}}(\zeta)$ as follows.

1) The Lyapunov function $V(\zeta)$ assumes its minimum value of 0 at the origin

$$V(0) = 0. \quad (36)$$

2) $V(\zeta)$ is a positive definite function because it is a quartic scalar function with the minimum at the origin.
3) The optimal feedback control law is zero at the origin, i.e., from (32)

$$P^*_{\text{ice}}(0) = 0. \quad (37)$$

4) The optimal control law (32) makes the origin $\zeta(t) = 0$ asymptotically stable when $P_{\text{req}} = 0$, by means of satisfying

$$\frac{\partial V}{\partial \zeta} \cdot (-k P^*_{\text{ice}}(\zeta)) < 0, \quad \zeta \ne 0. \quad (38)$$

To show (38), without loss of generality, instead of P_{ice}, we consider P_{batt} as new control variable [using (4) and (26) given that $P_{\text{req}} = 0$ in the control design]. Thus, (32) is rewritten as

$$P^*_{\text{batt}}\eta_{\text{mot}} = \begin{cases} -\dfrac{2k^2\left(\mu^4\zeta^3\right)^2}{\left(-k\mu^4\zeta^3 + \eta_{\text{mot}} n_1(\omega_{\text{mot}})\ g(t)\right)\gamma^2} & A \\ -\zeta^2 & B \end{cases} \quad (39)$$

with

$$A = \{\zeta > \bar{\zeta}^* \vee \zeta \le 0\}$$
$$B = \{0 < \zeta \le \bar{\zeta}^*\}$$

where $\bar{\zeta}^* = (-\eta_{\text{mot}} n_1(\omega_{\text{mot}})/k\mu^4)^{1/3}$. Thus (38) becomes

$$\mu^4 \cdot \zeta^3 \cdot k \cdot \eta_{\text{mot}} P^*_{\text{batt}}(\zeta) < 0, \quad \zeta \ne 0. \quad (40)$$

In the domain $0 < \zeta \le \bar{\zeta}^*$, it is immediate to see that

$$-\mu^4\ \zeta^3\ k\ \zeta^2 < 0. \quad (41)$$

In the domain $\zeta > \bar{\zeta}^* \vee \zeta \le 0$ the denominator of (40) is positive when ζ is positive and negative otherwise, thus leading to

$$\begin{cases} -\mu^4\zeta^3 k \cdot 2k^2(\mu^4\zeta^3)^2 < 0 & \zeta > \bar{\zeta}^* \\ \mu^4\zeta^3 k \cdot 2k^2(\mu^4\zeta^3)^2 < 0 & \zeta \le 0. \end{cases} \quad (42)$$

5) The Hamiltonian function (31) takes on the minimum value when the optimal control law (32) is applied. The shifted Hamiltonian $\bar{\mathcal{H}}$

$$\bar{\mathcal{H}}\left(\zeta, P^*_{\text{ice}}, \frac{\partial V}{\partial \zeta}\right) = \dot{m}_f + \Gamma(\zeta, P^*_{\text{ice}}) + \frac{\partial V}{\partial \zeta}(-k \cdot P^*_{\text{ice}}(\zeta)) \quad (43)$$

becomes

$$\bar{\mathcal{H}} = p_1 \cdot P_{\text{ice}} + \frac{1}{\gamma^2}k^2(\mu^4\zeta^3)^2\left(1 + \log\left(P^2_{\text{ice}}\right)\right)^2 + \mu^4\zeta^3(-k \cdot P_{\text{ice}}) \quad (44)$$

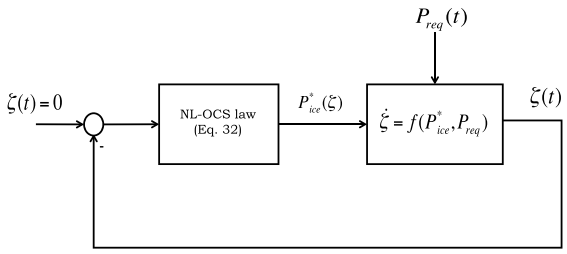

Fig. 8. NL-OCS-based control strategy scheme.

for the system (28) and cost function (29). It can be easily shown that the closed-loop controller (32) is a minimum of the $\bar{\mathcal{H}}$ (the stationary first-order conditions and the second-order convexity conditions are verified).

6) The passivity condition (condition 5 of Theorem 2) with respect to the disturbance input P_{req} requires the following inequality to be satisfied:

$$\left(\frac{\partial V}{\partial \zeta}\right)\cdot k\cdot P_{\text{req}} \leq r(\zeta, P_{\text{req}}) + \dot{m}_f + \Gamma(\zeta, P^*_{\text{ice}}). \quad (45)$$

A second-order algebraic inequality in P_{req} is obtained and it is verified by imposing the discriminant $\Delta \leq 0$. This leads to an upper bound on γ of $\bar{\gamma} = 2.369$.

Since all the sufficient conditions from Theorem 2 (in the Appendix) are being satisfied with the proposed optimal controller (32) then conditions 1 and 2 in Theorem 1 hold true. Hence, the origin $\zeta = 0$ of the closed-loop system is optimally locally asymptotically stable when $P_{\text{req}} = 0$. Moreover, P^*_{ice} is optimal with respect to the adjoint functional $\mathcal{J}(\zeta_0, P_{\text{ice}}(\cdot))$ (defined in (58)) which represents an upper bound for $J_\infty(\zeta_0, P_{\text{ice}}(\cdot))$.

Note that the optimal control law obtained from Theorem 1 assures that the SOE reaches its reference value, SOE_{ref}, following an optimal path leading to minimum fuel consumption. This strategy is implemented within the closed-loop system shown in Fig. 8 and it is referred to as NL-OCS. In the following sections, the results obtained by implementing the NL-OCS solution are shown and compared to the benchmark and real-time solutions provided by PMP and A-PMP, respectively.

VII. Benchmark and Real-Time Solution: PMP and A-PMP

In this section, we present an overview of the benchmark solution based on PMP used to validate the new control law. In general, the PMP gives a set of instantaneous necessary conditions for optimality, which are in turns used to find optimal control candidates [25].

The PMP states that the optimal control law $u^*(t)$ of Problem 1 must satisfy the following necessary conditions.

1) $u^*(t)$ minimizes at each instant of time the Hamiltonian associated to the system

$$\mathcal{H}(t, u(t), \zeta(t), \lambda(t)) = \lambda(t)\cdot\dot{\zeta}(t, u(t), \zeta(t)) + L(t, u(t), \zeta(t)) \quad (46)$$

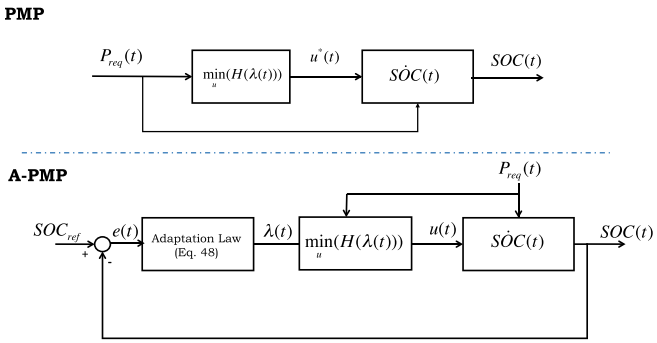

Fig. 9. Top: PMP-based control scheme. Bottom: A-PMP-based strategy control scheme.

with $\dot{\zeta}(t, u(t), \zeta(t))$ being the system dynamics equation, $L(u(t))$ being the instantaneous cost, and λ being a vector of auxiliary variables called adjoint state or costates of the system; λ has the same dimension as the state vector ζ, and therefore is a scalar in our problem.

2) The costate variable must satisfy the following dynamic equation:

$$\dot{\lambda} = -\left.\frac{\partial \mathcal{H}(t, u(t), \zeta(t), \lambda(t))}{\partial \zeta}\right|_{u^*, \zeta^*}. \quad (47)$$

In practical applications, the minimum principle can be used to find solution candidates by computing and minimizing the Hamiltonian function at each instant of time. This control problem is usually solved using an iterative procedure, known as the shooting method [24].

It is important to notice that the PMP-based controller operates in open loop, as shown in Fig. 9, and the control variable depends on the actual power request P_{req}, which enters in both blocks of minimization and plant dynamics. No information is fed-back to the optimizing controller.

In this paper, the PMP solution is a proxy for the global optimal solution and it is used as a benchmark solution for the proposed control strategy as it gives the theoretical optimum. In addition to the PMP, the evaluation of the proposed control design is performed also against a real-time implementable controller. In this paper, we choose the A-PMP to perform such an evaluation. The reason is twofold: 1) A-PMP, among the real-time implementable controllers [54], gives near-optimal performance [43] and 2) it is of straightforward implementation within the forward vehicle simulator used as it is based on the already implemented PMP. The A-PMP is a variant of PMP where the costate λ is adapted from feedback from SOC in real-time according to

$$\lambda(k) = \frac{\lambda(k-1) - \lambda(k-2)}{2} + K\cdot(\text{SOC}_{\text{ref}} - \text{SOC}(k)) \quad (48)$$

where k is an integer number indicating the kth fixed time interval of length T seconds, and the $\lambda(k)$ is the value of the costate in the interval $[(k-1)T, kT]$. The A-PMP-based energy management supervisory controller is implemented according to the scheme shown in Fig. 9.

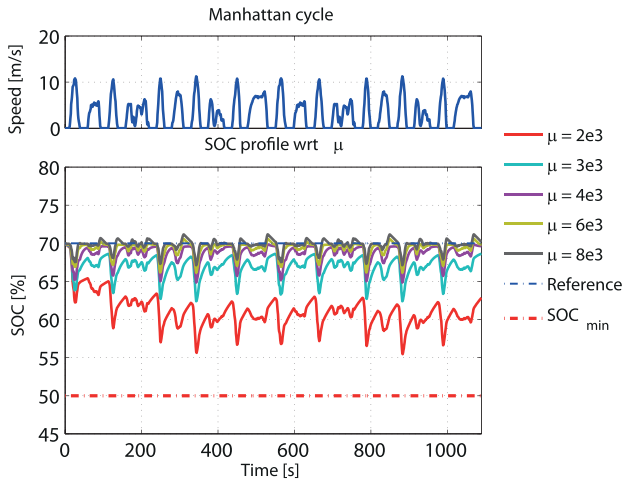

Fig. 10. SOC profiles from NL-OCS for different μ over the Manhattan Cyc.

VIII. Simulation Results

In this section, the implementation of the proposed control strategy is conducted over the vehicle PSAT model presented in Section III. Results are compared against the optimal solution provided by PMP and the real-time solution provided by the A-PMP for different driving scenarios. Moreover, a sensitivity study of the control strategy against the control parameter and driving characteristics is also conducted.

A. NL-OCS Parameter Calibration

In the optimal and stable control law (32) the values of k and $p_1(\omega_{\text{ice}})$ are known from the vehicle models, γ is a constant whose upper bound was obtained from the theorem's proof, whereas μ is the only calibration parameter that needs to be selected for on-board implementation. The calibration of μ is conducted in such a way the strategy performs near the optimum in real-time operation despite the driving conditions. From (32) one can see that μ ultimately affects the amount of fuel consumed over each driving Cyc, as the power requested from the engine is a function of μ. Fig. 10 shows the effect of different choices of μ within the domain set $F_\mu = [2 \cdot 10^3; 8 \cdot 10^3]$ on SOC.

The effect of μ on fuel economy and the final SOC are reported in the two plots of Fig. 11 for four different driving Cycs, where the quantities Δ SOC and the equivalent fuel consumption FC_{eq} are defined as follows:

$$\begin{cases} \Delta\text{SOC} = \dfrac{\text{SOC}(T) - \text{SOC}_{\text{ref}}}{\text{SOC}_{\text{ref}}} \\ \text{FC}_{\text{eq}} = \displaystyle\int_0^T \dot{m}_f \, dt + \Delta\text{SOC} \cdot \frac{E_{\max}}{\eta \cdot Q_{\text{LHV}}}. \end{cases} \tag{49}$$

The evaluation of FC_{eq} comes from two contributions: 1) the nominal computed fuel consumption and 2) the fuel consumption error due to the difference between the initial and final SOC values during a given driving scenario. In other words, this second-term considers the theoretical consumption, lost or saved, that there would be if the final SOC value did not reach its reference setpoint.

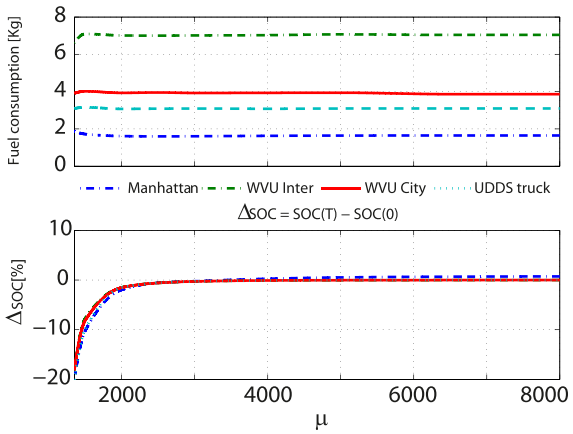

Fig. 11. Fuel consumption and Δ SOC with respect to μ for four different driving Cycs.

TABLE II
Control Law Sensitivity to μ Variation

	FC_{eq} [kg]	μ^*	ΔSOC
Manhattan	1.588	2.47e3	5.5e-2
WVU Inter	7.027	2.56e3	5.8e-2
WVU City	3.862	6.40e3	1.0e-3
UDDS truck	3.073	2.12e3	15.1e-2

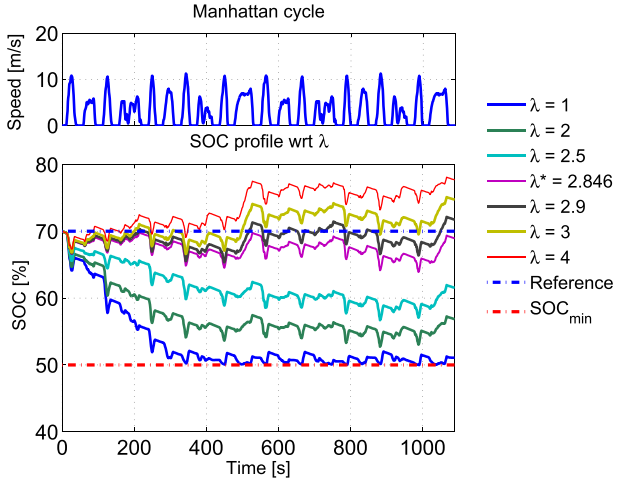

Fig. 12. SOC profiles from PMP for different values of λ over the Manhattan Cyc.

As one can observed from Fig. 11, the proposed control law shows low sensitivity against driving conditions for a wide range of values of μ (within the domain set F_μ). In Table II, the FC_{eq} and Δ SOC are reported for the four different driving Cycs used together with the optimal value of μ. In particular, charge-sustainability is guaranteed for a wide (and same) range of μ values despite the driving Cyc, as observed in the plot at the bottom of Fig. 11 where the four Δ SOC behaviors are almost completely overlapped.

As already known form the literature (e.g., [25], [42]), the PMP solution is very sensitive to the costate λ (which is the only parameter that needs to be calibrated). This is shown in Fig. 12, where different SOC trajectories are plotted as λ varies. Only one optimal value of λ exists, though that ensures charge-sustainability.

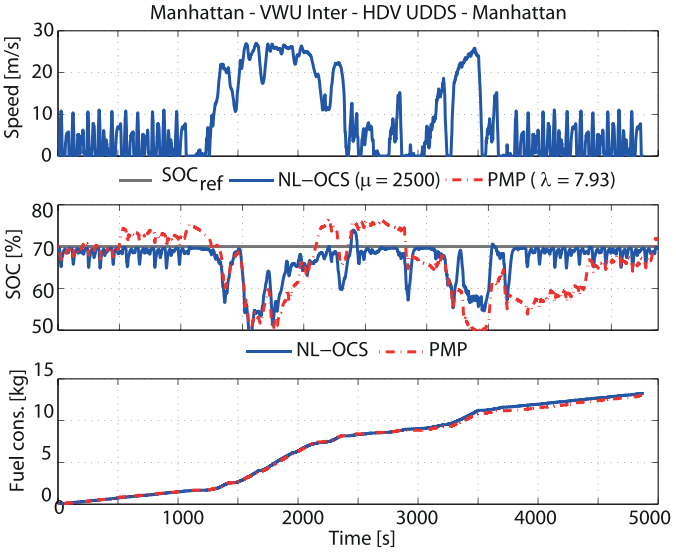

Fig. 13. Fuel consumption FC_{eq} and SOC profile for PMP and NL-OCS control strategies.

TABLE III

FUEL CONSUMPTION AND ENGINE EFFICIENCY COMPARISON FOR THE COMPOSITE DRIVING CYC OF FIG. 13

Controller	FC_{eq}[kg]	ICE eff.
PMP	13.11	0.319
NL-OCS	13.24	0.310

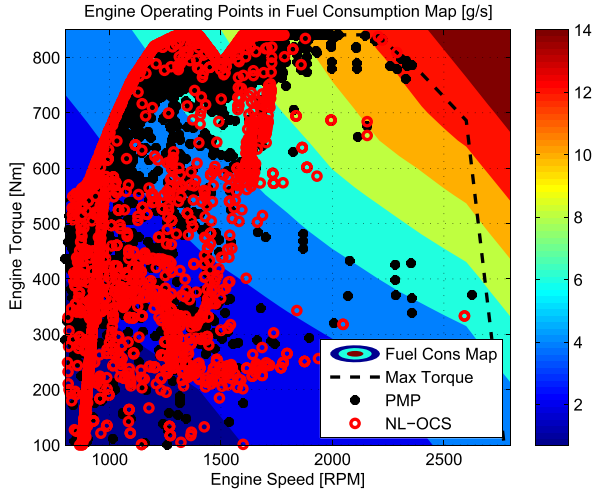

Fig. 14. Engine operating points over the combined driving Cyc: PMP and NL-OCS solutions.

A comparison of the performance of the NL-OCS control law (32) and the PMP solution is shown in Fig. 13 over a composite driving Cyc (obtained by concatenating Manhattan, west virginia urban (WVU) Interstate, heavy-duty urban dynamometer driving schedule, and Manhattan driving schedules).

Table III compares the fuel consumption and the engine efficiency of both control strategies (optimally tuned). It can be noticed that the solution obtained with NL-OCS is very close to the benchmark solution provided by PMP. If, on one hand, the closed-form control law consumes an average of 1% more fuel than the optimal solution, on the other hand it shows better capability to maintain the SOC close to the reference

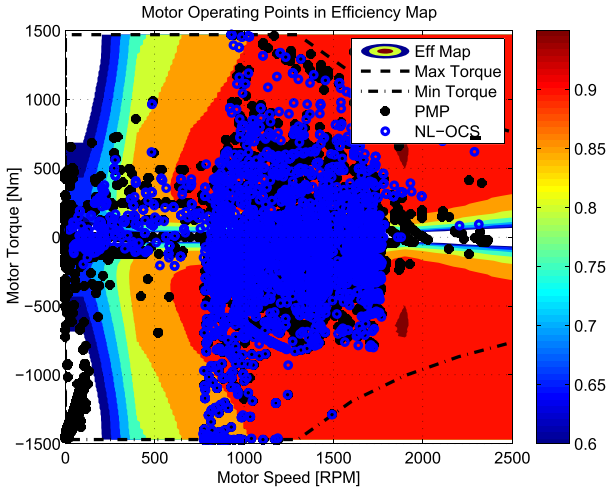

Fig. 15. Electric motor operating points over the combined driving Cyc: PMP and NL-OCS solutions.

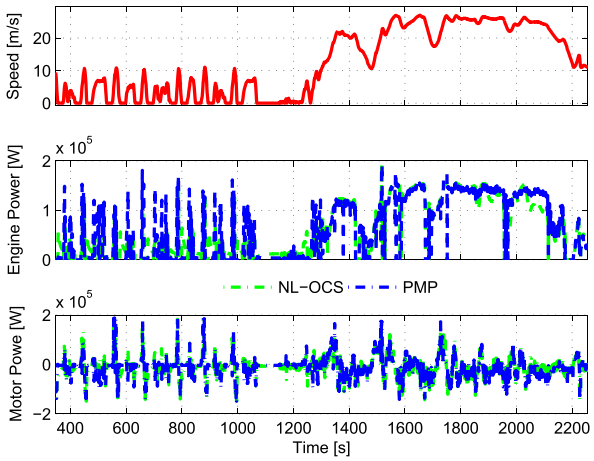

Fig. 16. Engine and electric motor power profiles (zoomed-in-view) from PMP and NL-OCS solutions.

TABLE IV

FUEL CONSUMPTION AND ENGINE EFFICIENCY COMPARISON FOR SINGLE DRIVING CYCS

Controller	FC_{eq}[kg]	ICE eff.
Manhattan		
PMP	1.579	0.318
NL-OCS	1.589	0.309
WVU-Inter		
PMP	6.998	0.359
NL-OCS	7.029	0.311
HD-UDDS		
PMP	3.066	0.356
NL-OCS	3.082	0.310

value SOC_{ref} (set to 0.7). The engine and the electric motor operate mostly in the same regions when the two strategies are running, as shown in Figs. 14 and 15. In Fig. 16, a zoomed-in-view of the engine power and motor power profile shows that the actuators behavior is very similar in the two cases.

A Cyc-by-Cyc comparison of the two strategies is shown in Table IV. Similarly to the case of composite driving Cyc, the NL-OCS performs very close to the PMP both in terms of fuel consumption and engine efficiency.

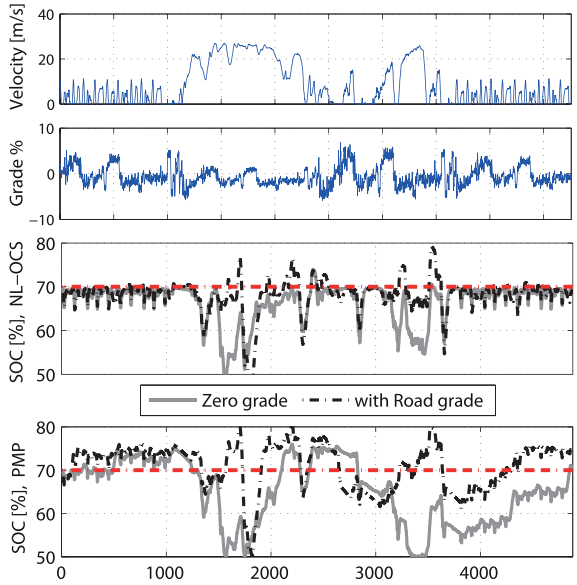

Fig. 17. SOC profiles from NL-OCS and PMP in case of zero-grade and with road grade.

TABLE V
SENSITIVITY ANALYSIS AGAINST BATTERY PARAMETERS VARIATION

	FC_{eq}^{PMP}	ΔFC_{eq}	FC_{eq}^{NL-OCS}	ΔFC_{eq}
R_{nom}, C_{nom}	**13.112**		**13.240**	
$R_{+5\%}$	13.261		13.306	
$R_{+10\%}$	13.348	+1.8%	13.385	+1.1%
$C_{-5\%}$	13.239		13.270	
$C_{-10\%}$	13.233		13.271	
$C_{-15\%}$	13.218	+0.01%	13.272	+0.002%
$C_{-20\%}$	13.203		13.272	
$R_{+10\%}$, $C_{-20\%}$	**13.235**	+1%	**13.308**	+0.51%

A sensitivity analysis of the proposed control strategy against both road conditions and battery parameters and comparison with PMP are conducted in the following.

Fig. 17 shows both the SOC profile from NL-OCS under zero grade and real grade pattern (from GNSS/GPS data, in terms of % slope), as well as the PMP solution under the same grade scenarios.

Because of the feedback mechanism from the SOC used in the NL-OCS supervisory controller, this strategy has a very low sensitivity to road grade variation as compared with the PMP solutions, which instead, operating in open loop have the tendency to diverge from the optimal solution obtained with zero-grade.

It is well known that the degradation in the battery manifests itself through resistance growth and capacity decrease [55]. Typically, OEMs define battery end-of-life as the moment in time when the capacity has reached 80% of its nominal value and/or resistance has increased of 10%. The sensitivity analysis conducted in this section aims at investigating the robustness of the proposed control law against battery parameters over battery life. The simulations are conducted for the same composite driving Cyc used earlier and both the battery capacity and the resistance are varied according to the values shown in Table V. Figs. 18 and 19 show the

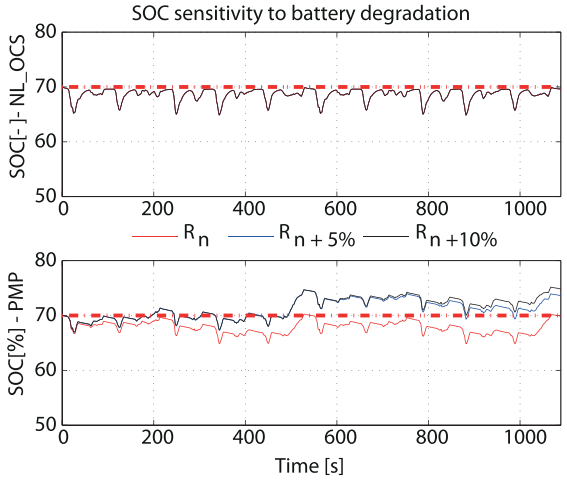

Fig. 18. SOC profiles from NL-OCS (top) and PMP (bottom) for increased values of resistance.

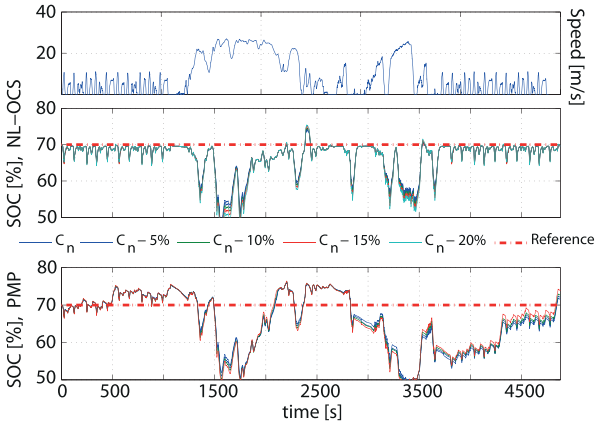

Fig. 19. SOC from NL-OCS (top) and PMP (bottom) for decreased values of capacity.

SOC trends of both strategies under: 1) resistance increase and 2) capacity decrease case. In particular, the simulation results from PMP were conducted using the optimal λ found when the nominal battery parameters (new battery) were used. As one can observe in Fig. 18, charge-sustainability is slightly compromised if a new costate value is not optimally found. Fig. 20 compares the SOC obtained from the two controllers in case of new battery and dead battery. As one can notice, although both strategies react quite satisfactorily in term of fuel saving loss, the NL-OCS ensures performance within 0.5%, while the PMP of 1%, as reported in Table V.

The analysis conducted thus far has shown the low parameter sensitivity of the novel supervisory controller under various driving and road conditions, as well as the system parameters. The results obtained from this analysis are used to calibrate the new analytical controller for real-time use. To validate and test its performance a comparison with A-PMP is provided to show the feasibility in real-time simulation.

The A-PMP is based on the feedback from the actual SOC (48) that adapts dynamically the value of the costate λ.

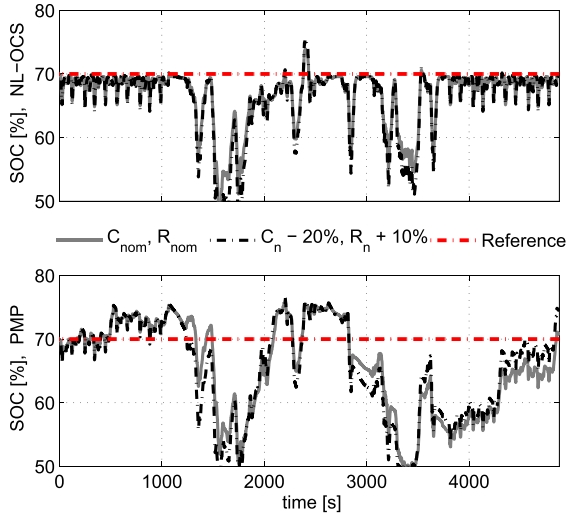

Fig. 20. SOC profiles from NL-OCS (top) and PMP (bottom) for nominal battery parameters ($C_{\text{nom}}, R_{\text{nom}}$) and end-of-life parameters ($C_{\text{nom}} - 20\%$, $R_{\text{nom}} + 10\%$).

TABLE VI
COMPARISON BETWEEN THE A-PMP AND NL-OCS SOLUTIONS FOR DIFFERENT DRIVING SCENARIOS

Controller	FC_{eq} [kg]
Manhattan	
A-PMP	1.592
NL-OCS	1.589
WVU-Inter	
A-PMP	6.037
NL-OCS	7.029
HD-UDDS	
A-PMP	3.075
NL-OCS	3.082
Composite cycle	
A-PMP	13.36
NL-OCS	13.24

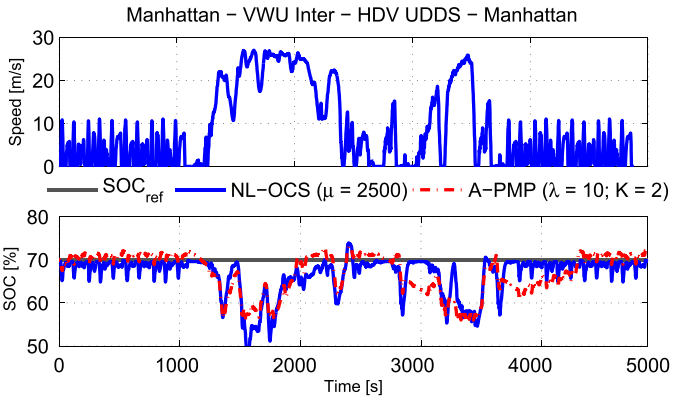

Fig. 21. SOC from A-PMP and NL-OCS control strategies.

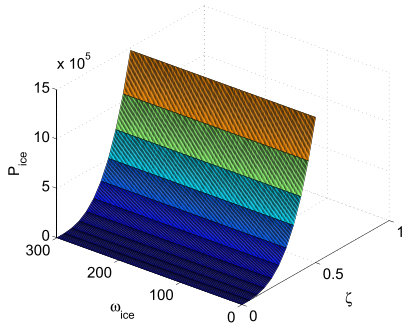

Fig. 22. Engine power map: $P_{\text{ice}} = f(\omega_{\text{ice}}, \zeta)$.

TABLE VII
COMPUTATION DEMAND COMPARISON [s]

Cycle	A-PMP$_{M_1}$	A-PMP$_{M_2}$	NL-OCS$_{M_1}$	NL-OCS$_{M_2}$
1 Cyc	140.17	84.61	30.17	21.35
2 Cyc	357.12	209.86	69.11	46.43
4 Cyc	626.02	379.16	154.69	73.01

The calibration of A-PMP is conducted via trial and error. The value of the proportional feedback gain is set to $K = 2$, $\lambda_0 = 10$ and the adaptation period is set to $T = 60$ s. The calibration of the NL-OCS on the other end is done on the basis of the sensitivity study presented earlier. A value of $\mu = 2.5 \cdot 10^3$ is selected.

Table VI reports the overall comparison between the two controllers showing that the fuel consumption in the two cases is very similar, at the price though of higher calibration effort needed for the A-PMP. Both strategies are capable to ensure charge-sustainability, as also shown in Fig. 21.

Besides the low calibration effort (along with the low sensitivity to the control parameter) the NL-OCS is well suited for fast computation. The power issued by the control law (32) can be mapped and computed offline as a function of the error ζ and engine speed ω_{ice}. As a result a lookup table is generated which is shown in Fig. 22.

All the simulation results shown so far were performed on two different machines:

1) *M_1:* Core i3@2.13 GHz 8Gb@1066 MHz ddr3;
2) *M_2:* Core i5@3.07 GHz 12Gb@1600 MHz ddr3;

to assess the computational improvement obtained with NL-OCS over PMP. Table VII shows that the NL-OCS is up to five times faster than A-PMP. The first column of the table indicates how many times (1, 2, or 4) the composite driving Cyc is executed.

IX. HARDWARE-IN-THE-LOOP SIMULATIONS

In this section, we present results from HIL simulations conducted to validate and verify the analytical energy management strategy proposed in this paper.

HIL simulation has been a corner stone for automotive control engineers in the last decade for control strategy development purposes [56]. HIL approach enables control engineers to tune control strategies before going to the final step of implementing them in the vehicle. The HIL stand used in this paper is shown in Fig. 23. It includes:

1) desktop to run the plant model in HIL (DS 1006 I/O board mounted on a DS 2202 Mid-Size plant);
2) laptop or Host-PC to run the controller model on the Microautobox (MAB) 2 (DS 1401/1501 type);

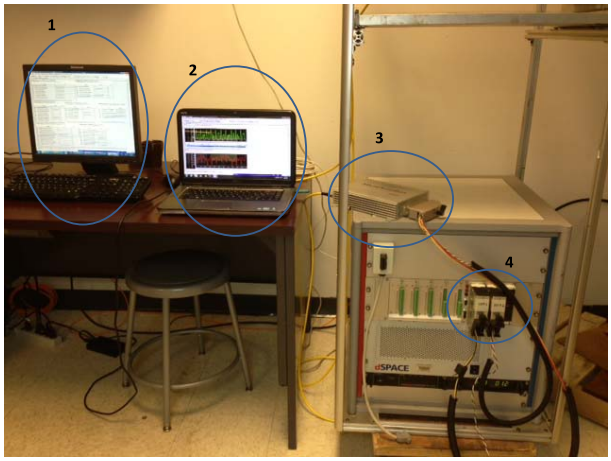

Fig. 23. HIL setup at the Ohio State University-Center for Automotive Research used in this paper.

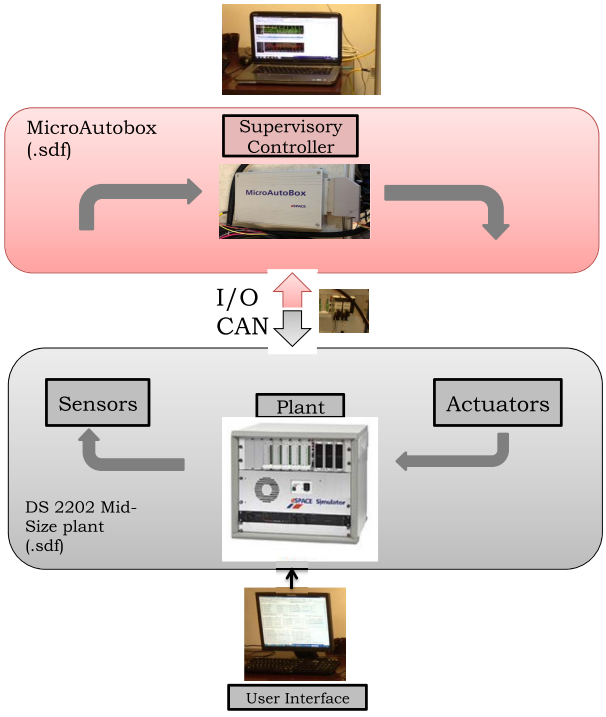

Fig. 24. HIL testing—schematic.

3) MAB connected to HIL plant via zero-insertion force connector;
4) HIL system (dSpace).

The vehicle model is flashed into the HIL system, while the supervisory controller is downloaded in the MAB. Connectors with the power and Controller Area Network (CAN) wiring to transmit signals (I/O CAN) are used to allow the communication between the two systems. The HIL setup schematic is shown in Fig. 24.

Fig. 25 shows the perfect velocity tracking of the HIL signal against the desired velocity, and Fig. 26 compares the SOC profiles from simulation and HIL. The performance obtained from the analytical solution implemented in HIL differs from the one obtained in Simulink by 1%.

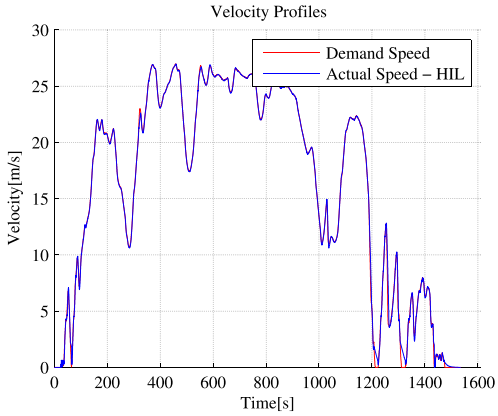

Fig. 25. HIL testing-speed tracking WVU Interstate Cyc.

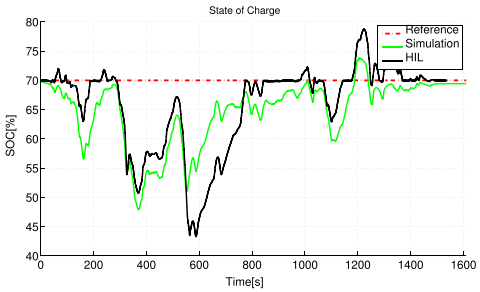

Fig. 26. HIL testing-SOC trajectory.

X. Conclusion

The novelty of this paper consists of rethinking the energy management problem in charge-sustaining HEVs as a nonlinear–nonquadratic infinite-time optimization problem. This approach leads to design a state-feedback-based control law that provides optimality with respect to an infinite time horizon performance functional, while guaranteeing asymptotic stability. In particular a Lyapunov-based dissipative approach is used to find the closed-form control law which is proven to be optimal with respect to the fuel consumption over an infinite-time horizon. The proposed optimal control law is implemented in a pre-transmission parallel hybrid heavy-duty vehicle and the performance of the closed-loop system is shown in simulation for different driving scenarios, and compared with the benchmark solution provided by PMP and the real-time solution provided by A-PMP. Results show very low sensitivity to the control parameter, low calibration effort, reduction of computational effort (up to five times faster than A-PMP), while maintaining the performance close to the optimal one (PMP) within 1%. HIL simulations were conducted to validate and verify the new strategy in a real-time simulation setup. To the best of our knowledge, this is the first time that an analytical closed-form solution (with guarantee of stability) was proposed to solve the energy management problem in HEVs and implemented in HIL environment.

Research is currently ongoing that aims at exploring possible extensions of the proposed control design to optimal control problems involving more than one state and one degree of freedom.

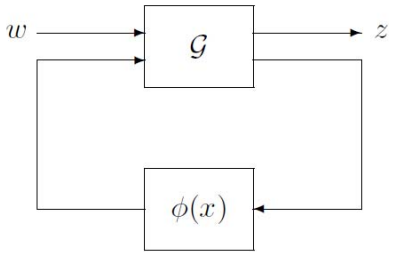

Fig. 27. Nonlinear closed-loop feedback system in presence of disturbance.

APPENDIX
LYAPUNOV-BASED APPROACH IN NONLINEAR OPTIMAL REGULATION

Let be $\mathcal{D} \subset \mathbb{R}^n$ an open set and let $\mathcal{U} \subset \mathbb{R}^m$, with $0 \in \mathcal{D}$ and $0 \in \mathcal{U}$. Moreover, let $\mathcal{W} \subset \mathbb{R}^d$. Consider now the controlled dynamical system

$$\begin{aligned} \dot{x}(t) &= F(x(t), u(t)) + G(x(t))w(t) \\ x(0) &= x_0, \quad w(\cdot) \in \mathcal{L}_2, \quad t \geq 0 \end{aligned} \tag{50}$$

with performance output vector

$$z(t) = h(x(t), u(t)) \tag{51}$$

where $F : \mathbb{R}^n \times \mathbb{R}^m \to \mathbb{R}^n$ satisfies $F(0, 0) = 0$, $G : \mathbb{R}^n \to \mathbb{R}^n \times \mathbb{R}^d$, $h : \mathbb{R}^n \times \mathbb{R}^m \to \mathbb{R}^p$ satisfies $h(0, 0) = 0$ and the control $u(\cdot)$ is restricted to the class of admissible controls such that $u(t) \in \mathcal{U}$, $\forall t \geq 0$. Given a feedback control law $u(t) = \phi(x(t))$, the closed-loop system shown in Fig. 27 has the form

$$\begin{aligned} \dot{x}(t) &= F(x(t), \phi(x(t))) + G(x(t))w(t) \\ x(0) &= x_0, \quad t \geq 0 z(t) = h(x(t), \quad \phi(x(t))). \end{aligned} \tag{52}$$

With respect to the open-loop system (50) and the closed one (52), the following assumptions and definitions are given.

Assumption 1: The mapping $\phi : \mathcal{D} \to \mathcal{U}$ satisfies sufficient regularity conditions such that the resulting closed-loop system (52) has a unique solution forward in time.

Let L: $\mathcal{D} \times \mathcal{U} \to \mathbb{R}$ and $\mathcal{S}$ be the set of regulation controllers for the nonlinear system with $w(t) \equiv 0$.

Definition 2: $\mathcal{S}(x_0) = \{u(\cdot)$: $u(\cdot)$ is admissible and such that $\dot{x}(t)$ given by (50), starting from initial state condition x_0, satisfies $x(t) \to 0$ as $t \to \infty$ with $w(t) \equiv 0\}$.

Definition 3: With respect to (50) and (51) and given a Lyapunov function $V : \mathcal{D} \to \mathbb{R}$, a positive storage function $\Gamma : \mathcal{D} \times \mathcal{U} \to \mathbb{R}$, and the given supply rate function $r : \mathbb{R}^p \times \mathbb{R}^d \to \mathbb{R}$ are introduced as follows:

$$\begin{cases} \Gamma(x, u) = \dfrac{1}{\gamma^2}\left(\dfrac{\partial V}{\partial x}\right)^2 f(u) \\ r(w, z) = \gamma^2 w^2 - z^2 \end{cases} \tag{53}$$

where $f(u)$ is a generic scalar nonlinear function of the control variable.

Definition 4: γ is the system $\mathcal{L}_2$ gain from w to z, representing the maximum energy amplification of the input signal $w \in \mathcal{L}_2$ on the performance variable z

$$\|z(\cdot)\|_2 \leq \gamma \|w(\cdot)\|_2. \tag{54}$$

Theorem 2 (From [49]): Consider the nonlinear dynamical system (50) and (51) with performance functional

$$J_\infty(x_0, u(\cdot)) = \int_0^\infty L(x(t), u(t))\, dt \tag{55}$$

where $u(\cdot)$ is an admissible control. Assume that there exist a Lyapunov function $V : \mathcal{D} \to \mathbb{R}$, a positive storage function $\Gamma : \mathcal{D} \times \mathcal{U} \to \mathbb{R}$, the given supply rate function $r : \mathbb{R}^p \times \mathbb{R}^d \to \mathbb{R}$, and a control law $\phi : \mathcal{D} \to \mathcal{U}$ such that

1. $V(0) = 0$
2. $V(x) > 0, \quad x \in \mathcal{D}, \quad x \neq 0$
3. $\phi(0) = 0$
4. $\dfrac{\partial V(x)}{\partial x} F(x, \phi(x)) < 0, \quad x \in \mathcal{D}, \quad x \neq 0$
5. $\dfrac{\partial V(x)}{\partial x} G(x) w \leq r(z, w) + L(x, \phi(x)) + \Gamma(x, \phi(x))$
   $x \in \mathcal{D}, \quad w \in \mathcal{W}$
6. $\begin{cases} \mathcal{H}(x, \phi(x)) = 0, \quad x \in \mathcal{D} \\ \mathcal{H}(x, u) \geq 0, \quad x \in \mathcal{D}, \quad u \in \mathcal{U} \end{cases}$ (56)

where

$$\mathcal{H}(x, u) = \frac{\partial V(x)}{\partial x} F(x, u) + L(x, u) + \Gamma(x, u). \tag{57}$$

Then:

1) there exists a neighborhood $\mathcal{D}_0 \subset \mathcal{D}$ of the origin such that the zero solution $x(t) \equiv 0$ of the undisturbed ($w(t) \equiv 0$) system is locally asymptotically stable;
2) if $x_0 \in \mathcal{D}_0$ then the feedback control $u(\cdot) = \phi(x(\cdot))$ minimizes $\mathcal{J}(x_0, u(\cdot))$ in the sense that

$$\mathcal{J}(x_0, \phi(x(\cdot))) = \min_{u(\cdot) \in \mathcal{S}(x_0)} \mathcal{J}(x_0, u(\cdot)) \tag{58}$$

where $\mathcal{J}(x_0, \phi(x(\cdot)))$ is the adjoint functional defined as

$$\mathcal{J}(x_0, u(\cdot)) = \int_0^\infty [L(x(t), u(t)) + \Gamma(x(t), u(t))] dt \tag{59}$$

and in addition

$$J_\infty(x_0, \phi(x(\cdot))) \leq \mathcal{J}(x_0, \phi(x(\cdot))) \tag{60}$$

3) if $\mathcal{D} = \mathbb{R}^n$, $\mathcal{U} = \mathbb{R}^m$, $w(t) \equiv 0$, and $V(x) \to \infty$ as $\|x\| \to \infty$, then the zero solution $x(t) \equiv 0$ of the closed-loop system is globally asymptotically stable.

Proof 2: The proof of Theorem 1 is given in [49, Ch. 10].

ACKNOWLEDGMENT

The authors would like to thank T. Mukherjee for his valuable contribution in conducting HIL experiments. T. Mukherjee was a M.S. student at Ohio State University at the time this work was conducted.

REFERENCES

[1] C. C. Chan, "The state of the art of electric and hybrid vehicles," *Proc. IEEE*, vol. 90, no. 2, pp. 247–275, Feb. 2002.

[2] J. Wahlström, L. Eriksson, and L. Nielsen, "EGR-VGT control and tuning for pumping work minimization and emission control," *IEEE Trans. Control Syst. Technol.*, vol. 18, no. 4, pp. 993–1003, Jul. 2010.

[3] L. Serrao, S. Onori, A. Sciarretta, Y. Guezennec, and G. Rizzoni, "Optimal energy management of hybrid electric vehicles including battery aging," in *Proc. Amer. Control Conf.*, Jun./Jul. 2011, pp. 2125–2130.

[4] D. F. Opila, X. Wang, R. McGee, R. B. Gillespie, J. A. Cook, and J. W. Grizzle, "An energy management controller to optimally trade off fuel economy and drivability for hybrid vehicles," *IEEE Trans. Control Syst. Technol.*, vol. 20, no. 6, pp. 1490–1505, Nov. 2012.

[5] F. Merz, A. Sciarretta, J.-C. Dabadie, and L. Serrao, "On the optimal thermal management of hybrid-electric vehicles with heat recovery systems," *Oil Gas Sci. Technol.-Rev. IFP Energies Nouvelles*, vol. 67, no. 4, pp. 601–612, 2012. [Online]. Available: http://dx.doi.org/10.2516/ogst/2012017

[6] L. Serrao *et al.*, "Open issues in supervisory control of hybrid electric vehicles: A unified approach using optimal control methods," *Oil Gas Sci. Technol.-Rev. IFP Energies Nouvelles*, vol. 68, no. 1, pp. 23–33, 2013. [Online]. Available: http://dx.doi.org/10.2516/ogst/2012080

[7] C. Lin, H. Peng, J. Grizzle, J. Liu, and M. Busdiecker, "Control system development for an advanced-technology medium-duty hybrid electric truck," in *Proc. TB–56, SAE Int. Truck Bus Conf.*, Nov. 2003.

[8] R. Mura, V. Utkin, and S. Onori, "Recasting the HEV energy management problem into an infinite-time optimization problem including stability," in *Proc. 52nd IEEE Annu. Conf. Decision Control*, Dec. 2013, pp. 6837–6842.

[9] P. Pisu and G. Rizzoni, "A comparative study of supervisory control strategies for hybrid electric vehicles," *IEEE Trans. Control Syst. Technol.*, vol. 15, no. 3, pp. 506–518, May 2007.

[10] A. Sciarretta and L. Guzzella, "Control of hybrid electric vehicles," *IEEE Control Syst.*, vol. 27, no. 2, pp. 60–70, Apr. 2007.

[11] F. R. Salmasi, "Control strategies for hybrid electric vehicles: Evolution, classification, comparison, and future trends," *IEEE Trans. Veh. Technol.*, vol. 56, no. 5, pp. 2393–2404, Sep. 2007.

[12] B. Mashadi and S. A. M. Emadi, "Dual-mode power-split transmission for hybrid electric vehicles," *IEEE Trans. Veh. Technol.*, vol. 59, no. 7, pp. 3223–3232, Sep. 2010.

[13] C. Mi, M. A. Masrur, and D. W. Gao, "Plug-in hybrid electric vehicles," in *Hybrid Electric Vehicles: Principles and Applications With Practical Perspectives*. New York, NY, USA: Wiley, 2011.

[14] B. M. Baumann, G. Washington, B. C. Glenn, and G. Rizzoni, "Mechatronic design and control of hybrid electric vehicles," *IEEE/ASME Trans. Mechatronics*, vol. 5, no. 1, pp. 58–72, Mar. 2000.

[15] C.-C. Lin, J.-M. Kang, J. W. Grizzle, and H. Peng, "Energy management strategy for a parallel hybrid electric truck," in *Proc. Amer. Control Conf.*, vol. 4. 2001, pp. 2878–2883.

[16] D. Bianchi *et al.*, "Layered control strategies for hybrid electric vehicles based on optimal control," *Int. J. Electr. Hybrid Veh.*, vol. 3, no. 2, pp. 191–217, 2011.

[17] R. Biasini, S. Onori, and G. Rizzoni, "A near-optimal rule-based energy management strategy for medium duty hybrid truck," *Int. J. Powertrains*, vol. 2, nos. 2–3, pp. 232–261, 2013.

[18] C.-C. Lin, H. Peng, J. W. Grizzle, and J.-M. Kang, "Power management strategy for a parallel hybrid electric truck," *IEEE Trans. Control Syst. Technol.*, vol. 11, no. 6, pp. 839–849, Nov. 2003.

[19] Y. Zhu, Y. Chen, G. Tian, H. Wu, and Q. Chen, "A four-step method to design an energy management strategy for hybrid vehicles," in *Proc. Amer. Control Conf.*, Jun./Jul. 2004, pp. 156–161.

[20] D. P. Bertsekas, *Dynamic Programming and Optimal Control*. Belmont, MA, USA: Athena Scientific, 1995.

[21] G. Delpart, S. Paganelli, T. M. Guerra, J. J. Santin, M. Delhorn, and E. Combes, "Algorithm optimization tool for the evaluation of HEV control strategies," in *Proc. Elect. Veh. Symp.*, vol. 16. Beijing, China, 1999.

[22] A. Piccolo, L. Ippolito, V. zo Galdi, and A. Vaccaro, "Optimisation of energy flow management in hybrid electric vehicles via genetic algorithms," in *Proc. IEEE/ASME Int. Conf. Adv. Intell. Mechatronics*, vol. 1. Jul. 2001, pp. 434–439

[23] H. P. Geering, *Optimal Control With Engineering Applications*. Berlin, Germany: Springer-Verlag, 2007.

[24] L. Serrao, S. Onori, and G. Rizzoni, "ECMS as a realization of Pontryagin's minimum principle for HEV control," in *Proc. Amer. Control Conf.*, Jun. 2009, pp. 3964–3969.

[25] L. Serrao, S. Onori, and G. Rizzoni, "A comparative analysis of energy management strategies for hybrid electric vehicles," *J. Dyn. Syst., Meas., Control*, vol. 133, no. 3, pp. 031012-1–031012-9, 2011.

[26] E. H. J. A. Nuijten *et al.*, "Advanced energy management strategies for vehicle power nets," in *Proc. 9th EAEC Int. Congr., Eur. Autom. Ind. Driving Global Changes*, Paris, France, 2003.

[27] M. Salman, M. Chang, and J. Chen, "Predictive energy management strategies for hybrid vehicles," in *Proc. IEEE Veh. Power Propuls. Conf.*, Chicago, IL, USA, Sep. 2005, pp. 21–25.

[28] H. Borhan, A. Vahidi, A. M. Phillips, M. L. Kuang, I. V. Kolmanovsky, and S. Di Cairano, "MPC-based energy management of a power-split hybrid electric vehicle," *IEEE Trans. Control Syst. Technol.*, vol. 20, no. 3, pp. 593–603, May 2012.

[29] L. Kolmanovsky, I. Siverguina, and B. Lygoe, "Optimization of powertrain operating policy for feasibility assessment and calibration: Stochastic dynamic programming approach," in *Proc. Amer. Control Conf.*, 2002, pp. 1425–1430.

[30] S. J. Moura, H. K. Fathy, D. S. Callaway, and J. L. Stein, "A stochastic optimal control approach for power management in plug-in hybrid electric vehicles," *IEEE Trans. Control Syst. Technol.*, vol. 19, no. 3, pp. 545–555, May 2011.

[31] G. Ripaccioli, A. Bemporad, F. Assadian, C. Dextreit, S. Cairano, and I. V. Kolmanovsky, "Hybrid modeling, identification, and predictive control: An application to hybrid electric vehicle energy management," in *Proc. 12th Int. Conf. Hybrid Syst., Comput., Control*, LNCS 5469. 2009, pp. 321–335.

[32] B. Sampathnarayanan, L. Serrao, S. Onori, G. Rizzoni, and S. Yurkovich, "Model predictive control as an energy management strategy for hybrid electric vehicles," in *Proc. 2nd Annu. Dyn. Syst. Control Conf.*, 2009, pp. 249–256.

[33] H. A. Borhan and A. Vahidi, "Model predictive control of a power-split hybrid electric vehicle with combined battery and ultracapacitor energy storage," in *Proc. Amer. Control Conf.*, 2009, pp. 3970–3976.

[34] M. Koot, J. T. B. A. Kessels, B. de Jager, W. P. M. H. Heemels, P. P. J. van den Bosh, and M. Steinbuch, "Energy management strategies for vehicular electric power systems," *IEEE Trans. Veh. Technol.*, vol. 54, no. 3, pp. 771–782, May 2005.

[35] A. Bemporad, M. Morari, V. Dua, and E. N. Pistikopoulos, "The explicit solution of model predictive control via multiparametric quadratic programming," in *Proc. Amer. Control Conf.*, 2000, pp. 872–876.

[36] Y. Wang and S. Boyd, "Fast model predictive control using online optimization," *IEEE Trans. Control Syst. Technol.*, vol. 18, no. 2, pp. 267–278, Mar. 2010.

[37] R. Milman and E. J. Davison, "A fast MPC algorithm using nonfeasible active set methods," *J. Opt. Theory Appl.*, vol. 139, no. 3, pp. 591–616, 2008.

[38] S. Di Cairano, W. Liang, I. V. Kolmanovsky, M. L. Kuang, and A. M. Phillips, "Power smoothing energy management and its application to a series hybrid powertrain," *IEEE Trans. Control Syst. Technol.*, vol. 21, no. 6, pp. 2091–2103, Nov. 2013.

[39] G. Paganelli, G. Ercole, A. Brahma, Y. Guezennec, and G. Rizzoni, "General supervisory control policy for the energy optimization of charge-sustaining hybrid electric vehicles," *JSAE Rev.*, vol. 22, no. 4, pp. 511–518, 2001.

[40] G. Paganelli, M. Tateno, A. Brahma, G. Rizzoni, and Y. Guezennec, "Control development for a hybrid-electric sport-utility vehicle: Strategy, implementation and field test results," in *Proc. Amer. Control Conf.*, 2001, pp. 5064–5069.

[41] N. Kim, S. Cha, and H. Peng, "Optimal control of hybrid electric vehicles based on Pontryagin's minimum principle," *IEEE Trans. Control Syst. Technol.*, vol. 19, no. 5, pp. 1279–1287, Sep. 2011.

[42] N. Kim and A. Rousseau, "Sufficient conditions of optimal control based on Pontryagin's minimum principle for use in hybrid electric vehicles," *Proc. Inst. Mech. Eng. D, J. Autom. Eng.*, vol. 226, no. 9, pp. 1160–1170, 2012.

[43] S. Onori, L. Serrao, and G. Rizzoni, "Adaptive equivalent consumption minimization strategy for hybrid electric vehicles," in *Proc. ASME Dyn. Syst. Control Conf.*, 2010, pp. 499–505.

[44] B. Gu and G. Rizzoni, "An adaptive algorithm for hybrid electric vehicle energy management based on driving pattern recognition," in *Proc. ASME Int. Mech. Eng. Congr. Expo.*, 2006, pp. 249–258.

[45] V. Sezer, M. Gokasan, and S. Bogosyan, "A novel ECMS and combined cost map approach for high-efficiency series hybrid electric vehicles," *IEEE Trans. Veh. Technol.*, vol. 60, no. 8, pp. 3557–3570, Oct. 2011.
[46] A. Sciarretta, M. Back, and L. Guzzella, "Optimal control of parallel hybrid electric vehicles," *IEEE Trans. Control Syst. Technol.*, vol. 12, no. 3, pp. 352–363, May 2004.
[47] D. S. Bernstein, "Nonquadratic cost and nonlinear feedback control," *Int. J. Robust Nonlinear Control*, vol. 3, no. 3, pp. 211–229, 1993.
[48] B. Sampathnarayanan, S. Onori, and S. Yurkovich, "An optimal regulation strategy for energy management of hybrid electric vehicles," in *Proc. 51st Annu. IEEE Conf. Decision Control*, Dec. 2012, pp. 7063–7068.
[49] W. M. Haddad and V. Chellaboina, *Nonlinear Dynamical Systems and Control*. Princeton, NJ, USA: Princeton Univ. Press, 2008.
[50] B. Sampathnarayanan, S. Onori, and S. Yurkovich, "An optimal regulation strategy with disturbance rejection for energy management of hybrid electric vehicles," *Automatica*, vol. 50, no. 1, pp. 128–140, 2014.
[51] *Powertrain System Analysis Toolkit (PSAT) Documentation*, Argonne National Laboratory, DuPage County, IL, USA, 2006.
[52] G. Steinmaurer and L. del Re, "Optimal energy management for mild hybrid operation of vehicles with an integrated starter generator," SAE Tech. Paper 2005-01-0280, 2005.
[53] D. W. Gao, C. Mi, and A. Emadi, "Modeling and simulation of electric and hybrid vehicles," *Proc. IEEE*, vol. 95, no. 4, pp. 729–745, Apr. 2007.
[54] S. Onori and L. Serrao, "On adaptive-ECMS strategies for hybrid electric vehicles," in *Proc. 2nd Int. Sci. Conf. Hybrid Electr. Veh. (RHEVE)*, 2011, pp. 6–7.
[55] M. Dubarry, V. Svoboda, R. Hwu, and B. Y. Liaw, "Capacity and power fading mechanism identification from a commercial cell evaluation," *J. Power Sour.*, vol. 165, no. 2, pp. 566–572, 2007.
[56] K. Patil, S. K. Molla, and T. Schulze, "Hybrid vehicle model development using ASM-AMESim-Simscape co-simulation for real-time HIL applications," SAE Tech. Paper 2012-01-0932, 2012.

Roberto Mura (S'13) received the B.Sc. and M.Sc. (*cum laude*) degrees in automation and control system engineering from the Politecnico di Milano, Milan, Italy, with a thesis on the design of estimation and control algorithms aimed at the active management of a hybrid-electric power-assisted bicycle. He is currently pursuing the Ph.D. degree in control system engineering with the Dipartimento di Elettronica, Informazione e Bioingegneria, Politecnico di Milano, with a focus on the active and robust control techniques for reducing rotor-induced vibrations in rotorcrafts and helicopters.

He has been a Visiting Scholar with the Center for Automotive Research, Ohio State University, Columbus, OH, USA, where he has been involved in the energy management problem of heavy-duty hybrid and fuel-cell vehicles, after he was a trainee with STMicroelectronics, Catania, Italy, from 2012 to 2013, with a focus on the synthesis of KF/EKF algorithms in GNSS/GPS applications.

Vadim Utkin (SM'96–F'04) received the Ph.D. degree from the Institute of Control Sciences, Moscow, Russia.

He joined the Institute of Control Sciences in 1960, where he was the Head of the Discontinuous Control Systems Laboratory from 1973 to 1994. He is currently a Professor of Electrical and Computer Engineering with Ohio State University, Columbus, OH, USA. He has held visiting positions at universities in the U.S., Germany, Italy, and Japan. The origins of some of the concepts in variable structure systems and sliding-mode control can be traced to him. His current research interests include control of infinite dimensional plants, sliding modes in discrete-time systems, and control of electric drives and engines.

Dr. Utkin was a recipient of the Lenin Prize (the Highest Scientific Award in Russia) in 1972. He is an Associate Editor of the *International Journal of Control* and the *ASME Journal of Dynamic Systems, Measurement, and Control*.

Simona Onori (M'05) joined the Automotive Engineering Department, Clemson University, in 2013 as an Assistant Professor. She received the Laurea (*summa cum laude*) degree in computer engineering from the University of Rome Tor Vergata, Rome, Italy, in 2003, the M.S. degree in electrical and computer engineering from the University of New Mexico, Albuquerque, NM, USA, in 2004, and the Ph.D. degree in control engineering from the University of Rome Tor Vergata, in 2007.

She was with IBM, Rome, from 2000 to 2002, and Thales-Alenia Space, Rome, in 2007. From 2007 to 2013, she was with the Center for Automotive Research, Ohio State University (OSU), Columbus, OH, USA, where she was a Lecturer with the Department of Mechanical and Aerospace Engineering from 2010 to 2012. Her background is in control system theory. Her current research interests include ground vehicle propulsion systems, including electric and hybrid electric powertrains, electrochemical energy storage systems, and aftertreatment systems with an emphasis on modeling, simulation, optimization, and feedback control design.

Dr. Onori is a member of the International Federation of Accountants, the American Society of Mechanical Engineers (ASME), and the Society of Automotive Engineers (SAE). She was a recipient of the 2012 Lumley Interdisciplinary Research Award from the College of Engineering, OSU, and the 2011 TechColumbus Outstanding Technology Team Award. She is currently an Associate Editor of the ASME American Control Conference and the Dynamic Systems and Control Conference, the IEEE Control Systems Society's Conference Editorial Board, and the *SAE International Journal of Advanced Powertrains*.